Semiclassical Molecular Dynamics Simulations of the Excited State Photodissociation Dynamics of H_2O in the A^1B_1 Band†

Yinghua Wu and Victor S. Batista*

Department of Chemistry, Yale University, P.O. Box 208107, New Haven, Connecticut 06520-8107

Received: March 20, 2002; In Final Form: June 3, 2002

The photodissociation dynamics of H_2O in the A^1B_1 band is investigated by implementing a recently developed time-sliced semiclassical initial value representation method (Burant, J. C.; Batista, V. S. *J. Chem. Phys.* **2002**, *116*, 2748). The capabilities of the computational method are explored as applied to calculations of partial and total photodissociation cross sections associated with highly excited vibrational states of H_2O. The direct comparison of our semiclassical results with full quantum mechanical calculations shows that the semiclassical approach is able to describe the H_2O spectroscopy and the overall photodissociation dynamics in excellent agreement with full quantum mechanical results.

I. Introduction

Understanding the molecular mechanisms that are responsible for broad and structureless spectroscopic bands of polyatomic systems (e.g., the A^1B_1 absorption band of water) is a central problem in chemical dynamics. These relaxation processes are ideally suited to detailed investigation using new advanced computational methods for describing quantum reaction dynamics. This paper reports the first application of a recently developed time-sliced (TS) semiclassical initial value representation (SC-IVR) method[1] to the description of a real photochemical reaction: the ultrafast photodissociation dynamics of H_2O in the first absorption band (A^1B_1),

$$H_2O(X^1A_1) + \hbar\omega \rightarrow H_2O(A^1B_1) \rightarrow H(^2S) + OH(X^2\Pi, n_j) \quad (1)$$

where ω is the photon frequency, and n_j represents the ro-vibrational state of the OH photofragment. The photodissociation reaction, introduced by eq 1, is ideal for exploring the capabilities of new computational methods because it has been extensively investigated both theoretically and experimentally.[2] Most of the previous studies have been motivated by the importance of such a reaction in atmospheric and interstellar chemistry. In addition, the underlying photochemical process constitutes a prototype model for ultrafast and direct dissociation for which accurate ab initio potential energy surfaces are readily available.[3,4]

In recent years, there has been significant progress in the development of a wide variety of computational methods for describing reaction dynamics, and various simulations have developed an understanding of the H_2O spectroscopy at a detailed molecular level, including the analysis of the total absorption spectrum at room temperature,[5] the rotational and vibrational state distributions of OH photofragments following the photolysis at 157 nm in the bulk and in a molecular beam,[6] the rotational OH distributions originating from the photodissociation of single, nondegenerate rotational states of water,[7−9] the Raman spectra for H_2O, HOD and D_2O for several excitation wavelengths,[10] and the branching ratios for producing H and D atoms in the photodissociation of HOD at 157 nm.[11] All experimental results have been very well reproduced and explained by the various theoretical calculations.

The relaxation dynamics that follows photoexcitation of H_2O molecules initially prepared in the ground vibrational state was found to be relatively simple and has been successfully modeled in terms of classical molecular dynamics simulations.[9,12] However, the photodissociation from highly excited vibrational states required a rigorous quantum mechanical treatment[4,13−15] (e.g., earlier SC-IVR simulations have been only partially successful at reproducing full quantum mechanical results[16]). It is, therefore, of interest to explore to what extent a more accurate semiclassical method (e.g., the TS SC-IVR of ref 1) is able to describe the photodissociation dynamics of H_2O, prepared in highly excited vibrational states. In particular, we would like to test the capabilities of the method as applied to describe the absorption spectra and the final product distributions that result from the photodissociation of the $|40^-\rangle$ and $|31^-\rangle$ vibrational states. These states have been studied both experimentally[17] and theoretically,[15] and they are almost degenerate, each containing roughly four quanta of OH vibration. Remarkably, however, they relax according to different photodissociation pathways (e.g., the $|40^-\rangle$ state produces almost exclusively OH ($n = 0$), for photoexcitation energies near the onset of the spectrum, whereas the dissociation of the $|31^-\rangle$ state yields primarily OH ($n = 1$), where n is the vibrational quantum number).

SC-IVR methods originated more than 30 years ago as a way of describing quantum dynamics according to classical molecular dynamics simulations.[18] In recent years, there has been considerable interest in the development of new implementation methods[16,19−31] that pursue the establishment of truly convenient alternatives to full-quantum mechanical techniques. The new implementation methodologies have been implemented in a number of model test systems and also in simulations of realistic reactions that allowed for direct comparisons with experimental data.[16,32−35] We have also applied the SC-IVR to simulations of realistic two-color pump−probe experiments of femtosecond photoelectron spectroscopy,[36] simulations of ultrafast photoinduced proton-transfer reactions,[37,38] and simulations of coherent control.[39,40]

† Part of the special issue "John C. Tully Festschrift".

10.1021/jp0207735 CCC: $22.00
Published on Web 07/16/2002

Of particular interest in this paper is the time-sliced semiclassical approach of reference.[1] The method computes the time evolution operator by concatenating finite time propagators along the lines of previous proposals,[30,41−51] and bridges the gap between semiclassical and full quantum dynamics because it becomes exact in the limit of sufficiently short time slice intervals. Reference 1 shows that the concatenation of finite time propagators significantly improves the accuracy of simulations based on the Herman−Kluk (HK) SC-IVR.[52] Although the method has yet to be applied to quantum dynamics simulations of real molecular systems, quantitative agreement with full quantum mechanical results has already been verified in the description of one- and two-dimensional model systems that included tunneling between disjoint classically allowed regions, long-time dynamics, and nonadiabatic dynamics. This paper, thus, reports the first application of the method to the computation of photodissociation cross sections of a real photochemical reaction.

The paper is organized as follows: section II outlines the semiclassical approach and its implementation to describe the H_2O dynamics of photodissociation, and the calculations of photodissociation cross sections. Section III describes our results and compares them with full quantum mechanical calculations. Section IV summarizes and concludes.

II. Semiclassical Approach

The details of the time-sliced semiclassical approach are readily available in ref 1. This section briefly describes the method in order to outline its implementation to model the excited-state photodissociation dynamics of H_2O.

The time-dependent wave function $\langle \mathbf{x}|\Psi_t(j)\rangle$ is obtained by propagating the initial state $|\Psi_0(j)\rangle$ according to

$$\langle \mathbf{x}|\Psi_t(j)\rangle = \int d\mathbf{x}'\, \langle \mathbf{x}|K_t|\mathbf{x}'\rangle\langle \mathbf{x}'|\Psi_0(j)\rangle \tag{2}$$

where $\mathbf{x}$ denotes the nuclear degrees of freedom, and $\langle \mathbf{x}|K_t|\mathbf{x}'\rangle$ is the time evolution operator in the coordinate representation

$$\langle \mathbf{x}|K_t|\mathbf{x}'\rangle \equiv \langle \mathbf{x}|e^{-i\hat{H}t/\hbar}|\mathbf{x}'\rangle \tag{3}$$

The time evolution operator, introduced by eq 3, is time-sliced by repeatedly inserting the resolution of identity

$$\hat{1} = \int d\mathbf{x}\, |\mathbf{x}\rangle\, \langle \mathbf{x}| \tag{4}$$

yielding

$$\langle \mathbf{x}_n|e^{-i\hat{H}(t_n-t_0)/\hbar}|\mathbf{x}_0\rangle = \int d\mathbf{x}_{n-1} \ldots \int d\mathbf{x}_1\, \langle \mathbf{x}_n|e^{-(i/\hbar)\hat{H}(t_n-t_{n-1})}|\mathbf{x}_{n-1}\rangle \ldots \langle \mathbf{x}_1|e^{-(i/\hbar)\hat{H}(t_1-t_0)}|\mathbf{x}_0\rangle \tag{5}$$

where $t_0 < t_1 < \ldots < t_{n-1} < t_n$. For sufficiently short time periods, $\tau = t_k - t_{k-1}$, each propagator introduced by eq 5 is approximated by the semiclassical propagator in its coherent-state representation[52]

$$e^{-(i/\hbar)\hat{H}\tau} \approx (2\pi\hbar)^{-D} \int d\mathbf{p}_0 \int d\mathbf{q}_0\, |\mathbf{p}_\tau,\mathbf{q}_\tau\rangle C_\tau(\mathbf{p}_0,\mathbf{q}_0) e^{iS\tau(p_0,q_0)/\hbar} \langle \mathbf{p}_0,\mathbf{q}_0| \tag{6}$$

where D is the number of nuclear degrees of freedom and $|\mathbf{p}_\tau,\mathbf{q}_\tau\rangle$ are the minimum uncertainty wave packets, or coherent states (CS),

$$\langle \mathbf{x}|\mathbf{p}_\tau,\mathbf{q}_\tau\rangle = \left(\frac{2\gamma}{\pi}\right)^{D/4} \exp[-\gamma(\mathbf{x}-\mathbf{q}_\tau)^2 + i\mathbf{p}_\tau(\mathbf{x}-\mathbf{q}_\tau)/\hbar] \tag{7}$$

The constant parameter γ introduced by eq 7 is the width of the coherent state. The integration variables $(\mathbf{p}_0, \mathbf{q}_0)$ in eq 6 are the initial conditions for classical trajectories of the time-evolved coordinates and momenta $\mathbf{q}_\tau \equiv \mathbf{q}_\tau(\mathbf{p}_0,\mathbf{q}_0)$ and $\mathbf{p}_\tau \equiv \mathbf{p}_\tau(\mathbf{p}_0,\mathbf{q}_0)$. These trajectories are obtained by integrating the usual classical equations of motion. The initial conditions $(\mathbf{p}_0, \mathbf{q}_0)$ define a basis set of regularly spaced coherent states for which $|\langle \mathbf{p}_0,\mathbf{q}_0|\Psi_0(j)\rangle| \geq \zeta$. The parameter ζ is determined by the desired accuracy. The basis set is reinitialized after each propagation time slice interval τ, using the truncation condition determined by the cutoff parameter ζ. $S_\tau(\mathbf{p}_0,\mathbf{q}_0)$ is the classical action along each trajectory, obtained by integrating the equation

$$\dot{S}_t = \mathbf{p}_t\cdot\dot{\mathbf{q}}_t - H(\mathbf{p}_t,\mathbf{q}_t) \tag{8}$$

for time τ. Finally, the preexponential factor $C_\tau(\mathbf{p}_0,\mathbf{q}_0)$ in eq 6 involves the monodromy matrix elements that are propagated according to the equations for the stability matrix.[52] The exact Hamiltonian operator in terms of Jacobi coordinates is given by

$$\hat{H} = -\frac{1}{2m}\left(\frac{\partial^2}{\partial R^2} + \frac{2}{R}\frac{\partial}{\partial R} - \frac{\mathbf{l}^2}{R^2}\right) - \frac{1}{2\mu}\left(\frac{\partial^2}{\partial r^2} + \frac{2}{r}\frac{\partial}{\partial r} - \frac{\mathbf{j}^2}{r^2}\right) + V(R,r,\theta) \tag{9}$$

where m and μ are the reduced masses for H_2O and OH, respectively. $\mathbf{l}$ is the orbital angular momentum of H with respect to OH and $\mathbf{j}$ is the molecular angular momentum of OH. $V(R,r,\theta)$ is the ab initio potential energy surface that describes the $\tilde{A}$ electronic excited state of H_2O,[3] and $\cos(\theta) = \mathbf{R}\cdot\mathbf{r}/Rr$.

To make a rigorous comparison with previous full quantum mechanical calculations by Schinke and co-workers,[4] as well as with previous SC-IVR results by Brumer and co-workers,[16] we consider the light−heavy−light (LHL) approximation where the hydrogen mass is negligible compared to the mass of oxygen. The approximation simply equates r and R to the two OH bond distances and is quite accurate for H_2O. Furthermore, bending motion is neglected, and the system is assumed to have total angular momentum $\mathbf{j} = 0$. Note that within the assumed approximations $\mu = m = m_H$, where m_H is the mass of a hydrogen atom, and the Hamiltonian assumes the form

$$H(r,R,P_R,p_r;\theta) = \frac{P_R^{\,2}}{2\mu} + \frac{p_r^{\,2}}{2m} + V(r,R,\theta) \tag{10}$$

To compare with calculations by Schinke[4] and Brumer,[16] we consider propagation on the $\tilde{A}$ state potential for $\theta = 104°$.

The total photodissociation cross sections $\sigma_j(E)$, as a function of the photon energy E, are obtained from the Fourier transform of the survival amplitude $\xi_j(t)$,

$$\sigma_j(E) = \frac{1}{2\pi\hbar}\int_{-\infty}^{\infty} dt\, \xi_j(t) e^{i(E_j+E)t/\hbar} \tag{11}$$

with

$$\xi_j(t) \equiv \langle \Psi_0(j)|e^{-i\hat{H}t/\hbar}|\Psi_0(j)\rangle = \langle \Psi_0(j)|\Psi_t(j)\rangle \tag{12}$$

Here, $|\Psi_0(j)\rangle = \mu_{\tilde{A}\tilde{X}}|j\rangle$ is the eigenstate $|j\rangle$ of energy E_j associated with the ground electronic state $\tilde{X}$ multiplied by the transition moment $\mu_{\tilde{A}\tilde{X}}$. Note that for simplicity (and likewise in the expressions of partial photodissociation cross sections) we do not include the frequency factor in the expression of the total photodissociation cross section. The $\tilde{A}$ excited-state potential energy surface and the transition moment $\mu_{\tilde{A}\tilde{X}}$ are parametrized

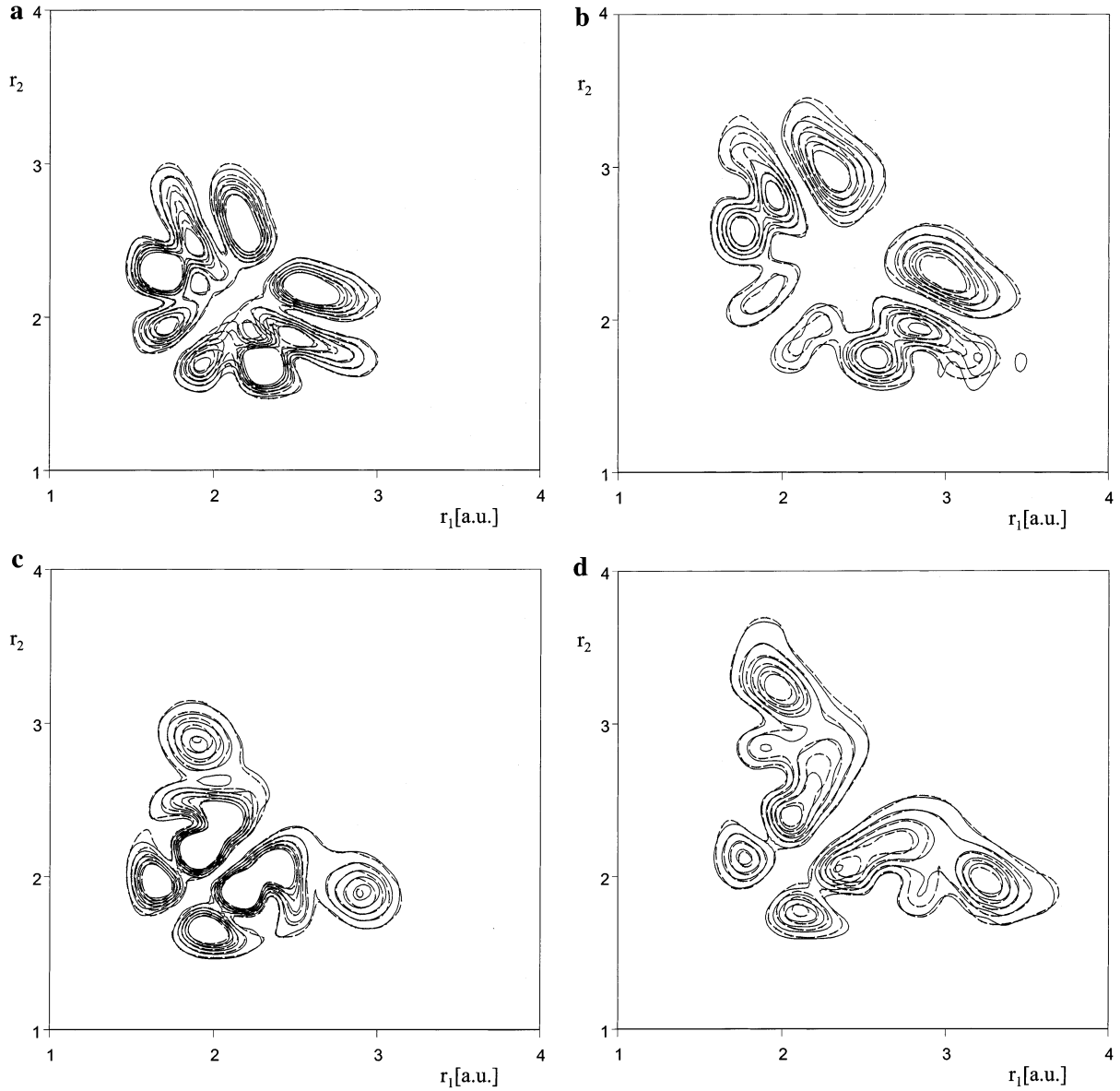

Figure 1. Contour plots for the norm of the time-evolved wave packet $|\Psi_t|$ versus the two OH separations r_1 and r_2 at 2.42 fs (panels a and c) and 3.63 fs (panels b and d) after photoexcitation of H_2O to the $\tilde{A}^1B_1$ electronic excited state. Results obtained according to the semiclassical methodology are displayed in solid lines. The corresponding full-quantum mechanical results are displayed in dashed lines. Panels a and b show results associated with the $|31^-\rangle$ initial state. Panels c and d show the analogous results for H_2O initially prepared in the $|40^-\rangle$ vibrational state.

according to ref 4 as described in sections II and IV, respectively. The initial vibrational states $|j\rangle$ in the calculations reported in section III are specified by the quantum numbers of excitation n and m, associated with the two OH stretching modes. We investigate the $|40^-\rangle$ and $|31^-\rangle$ states, which are the fifth ($j = 5$) and sixth ($j = 6$) eigenstates of ungerade symmetry. These states are obtained by computing the DVR eigenstates[53] of the $\tilde{X}$ empirical potential of Sorbie and Murrell.[54] Their corresponding energies with respect to the ground state are $E_5 = 13\,830.9$ cm^{-1} and $E_6 = 14\,318.8$ cm^{-1}.[55]

Partial photodissociation cross sections are obtained according to the quantum formalism due to Balint-Kurti et. al.,[56] where it is shown that the partial photodissociation cross sections $\sigma_n(E;j)$ are obtained from the Fourier transform

$$\sigma_n(E;j) = (2\pi)^{-1}\int_0^\infty \mathrm{d}t\, C_{j\rightarrow n}(R_\infty,t)\mathrm{e}^{\mathrm{i}(E+E_j)t/\hbar} \qquad (13)$$

with

$$C_{j\rightarrow n}(R_\infty,t) = \int_0^\infty \mathrm{d}r\, \langle\psi_n|r\rangle\langle r,R_\infty|\mathrm{e}^{-\mathrm{i}\hat{H}t/\hbar}|\Psi_0(j)\rangle \qquad (14)$$

where $|\psi_n\rangle$ are the asymptotic vibrational states of the OH photofragment. These vibrational states are numerically obtained according to the Numerov's method,[57] implemented on the ground-state potential energy surface[54] at $R = R_\infty = 6.0$ Å.

III. Results

Results are presented as follows. First, the semiclassical results for the individual wave packet components for both the $|40^-\rangle$ and the $|31^-\rangle$ initial states are compared to the corresponding quantum mechanical results. Such a comparison provides a comprehensive picture of the dependence of the survival amplitudes and photodissociation cross sections on the structure of nodes associated with the individual wave packets. The comparison also demonstrates the ability of the semiclassical methodology to describe *all* the features associated with the relaxation process after photoexcitation of the system.

Furthermore, an exhaustive comparison between semiclassical and full quantum mechanical results is presented for the total and partial photodissociation cross sections, as well as for their corresponding survival amplitudes associated with the $|00^+\rangle$, $|40^-\rangle$, and $|31^-\rangle$ initial states of H_2O, and the $|00^+\rangle$, $|01^-\rangle$, and $|10^-\rangle$ initial states of DOH. The comparison demonstrates that the TS SC-IVR of ref 1 is able to describe the H_2O spectroscopy as well as the complete photodissociation dynamics, including the isotopic substitution effects, in excellent agreement with full quantum mechanical calculations.

The semiclassical results were obtained by implementing a discretization of the basis defined by the spacings, $\Delta q_j = \sqrt{2/\gamma_j}$ and $\Delta p_j = \sqrt{\gamma_j}$, where the coherent state widths $\gamma_j = m_H\omega_j$, with $\omega_1 = 3671$ cm^{-1} (symmetric stretch) and $\omega_2 = 3759$ cm^{-1} (antisymmetric stretch), respectively. The calculations were obtained by using a cutoff parameter $\zeta = 10^{-5}$, resulting in a basis set that ranged from 2000 to 4500 coherent states throughout the whole propagation time. The reinitialization time slice interval $\tau = 3.0$ au. Full quantum mechanical results were obtained using the fast Fourier transform method[58] with an extended grid of 256 points in both the r and R Jacobi coordinates (i.e., a total of 65 536 grid points), defined in the range of coordinates $|X - 4.0 \text{ au}| < 3.0$ au, where $X = R, r$.

Figure 1 shows contour plots of the time evolved H_2O wave packet, initially prepared in the $|31^-\rangle$ state (see panels a and b), and in the $|40^-\rangle$ vibrational state (see panels c and d), respectively. The minus indicates that these states are antisymmetric with respect to the line defined by equal O−H distances. Panels a and c show the time-evolved wave packets at 2.42 fs, and panels b and c display wave packets at 3.63 fs. The comparison of our quantum results with previous quantum mechanical calculations (e.g., see Figure 2 of ref 15) indicates that the agreement is excellent. Also Figure 1 shows that the semiclassical results obtained according to the TS SC-IVR are in much better agreement with full quantum mechanical calculations than those reported by earlier SC-IVR computations (e.g., see Figure 1 of ref 16).

Figure 2a shows the comparison of survival amplitudes computed semiclassically (solid lines) and according to quantum mechanics (dashed lines). Results are shown for the H_2O molecule initially prepared in the $|31^-\rangle$ and $|40^-\rangle$ vibrational states, respectively. The agreement between semiclassical and quantum calculations is once again very satisfactory. These results are also in excellent agreement with previous quantum mechanical calculations (see Figure 3 of ref 15). The structures superimposed to the ultrafast decays in the $|31^-\rangle$ and $|40^-\rangle$ curves are due to the nodal structure in the initial wave packets (see Figure 1) and are therefore modulated by the partial overlap between the time-evolved wave function and the wave packet at time zero. For comparison, Figure 2a shows the survival amplitude for H_2O initially prepared in the $|00^+\rangle$ ground vibrational state.

The ultrafast decays give rise to the broad photodissociation cross sections displayed in Figure 2b as a function of the energy $E = E_j + \hbar\omega$ in the excited electronic state. As above, semiclassical results (solid lines) are compared to quantum (dashed lines) calculations. Throughout this paper energy normalization is such that $E = 0$ corresponds to the three separated ground-state atoms, H + H + O. The photodissociation cross section of the $|00^+\rangle$ state is much narrower and structureless, with slight modulations from a weak recurrence at 19 fs. These results are in excellent agreement with the full quantum calculations reported in Figure 4 of ref 15. Earlier SC-IVR calculations, however, were in only partial agreement with full quantum results.

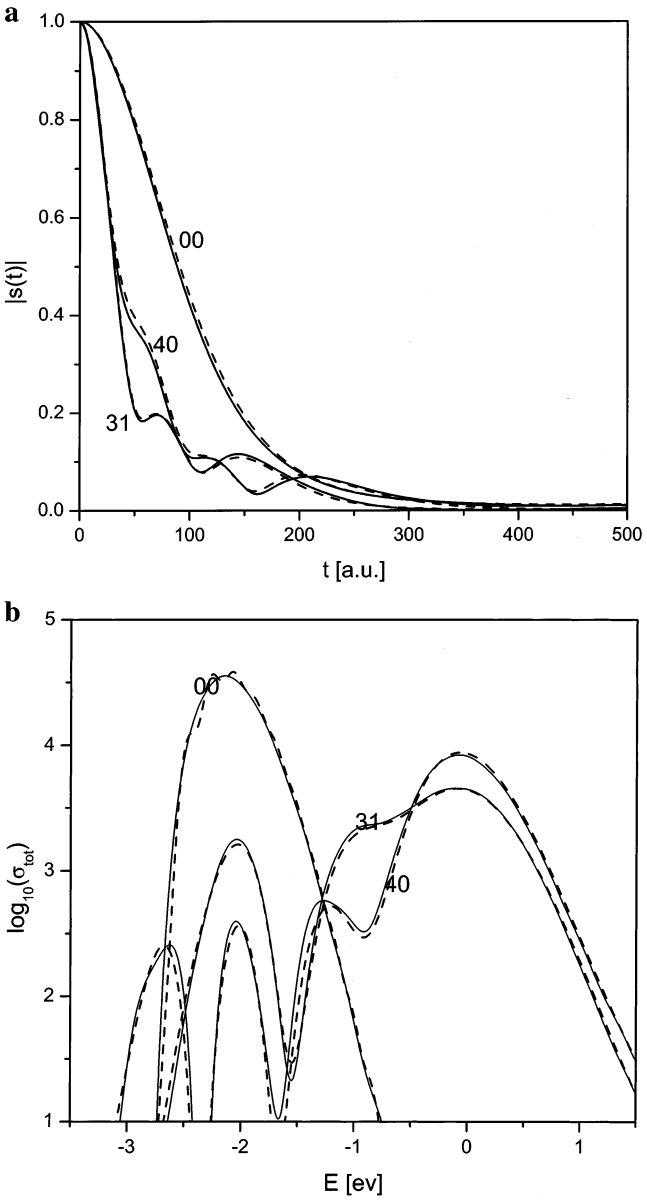

Figure 2. (a) Comparison of the semiclassical (solid lines) and the full quantum mechanical calculations (dashed lines) of the modulus of the survival amplitudes associated with the H_2O molecule initially prepared in the $|00^+\rangle$, $|31^-\rangle$, and $|40^-\rangle$ vibrational states for the first 500 au of dynamics. (b) Comparison of the semiclassical (solid lines) and quantum results (dashed lines) for the total photodissociation cross sections as a function of the energy $E = E_j + \hbar\omega$ in the excited electronic state, for H_2O initially prepared in the $|00^+\rangle$, $|31^-\rangle$, and $|40^-\rangle$ vibrational states. Note that photodissociation cross sections are in arbitrary units, and logarithmic scale to facilitate the comparison.

Figure 3 displays the partial photodissociation cross sections for the vibrational states $n = 0$, 1, and 2 of the OH photofragment. Panels a−c correspond to the H_2O molecule initially prepared in the $|00^+\rangle$, $|31^-\rangle$, and $|40^-\rangle$ vibrational states, respectively. These photodissociation cross sections are even more structured than the total photodissociation cross sections. The comparison between quantum and semiclassical results, however, is once again very satisfactory. It is very clear from Figure 3 that both quantum and semiclassical calculations are able to predict that the $|40^-\rangle$ state produces almost exclusively OH ($n = 0$), for energies between −2.5 and −1.5 eV, whereas the dissociation of the $|31^-\rangle$ state yields preferentially OH (n

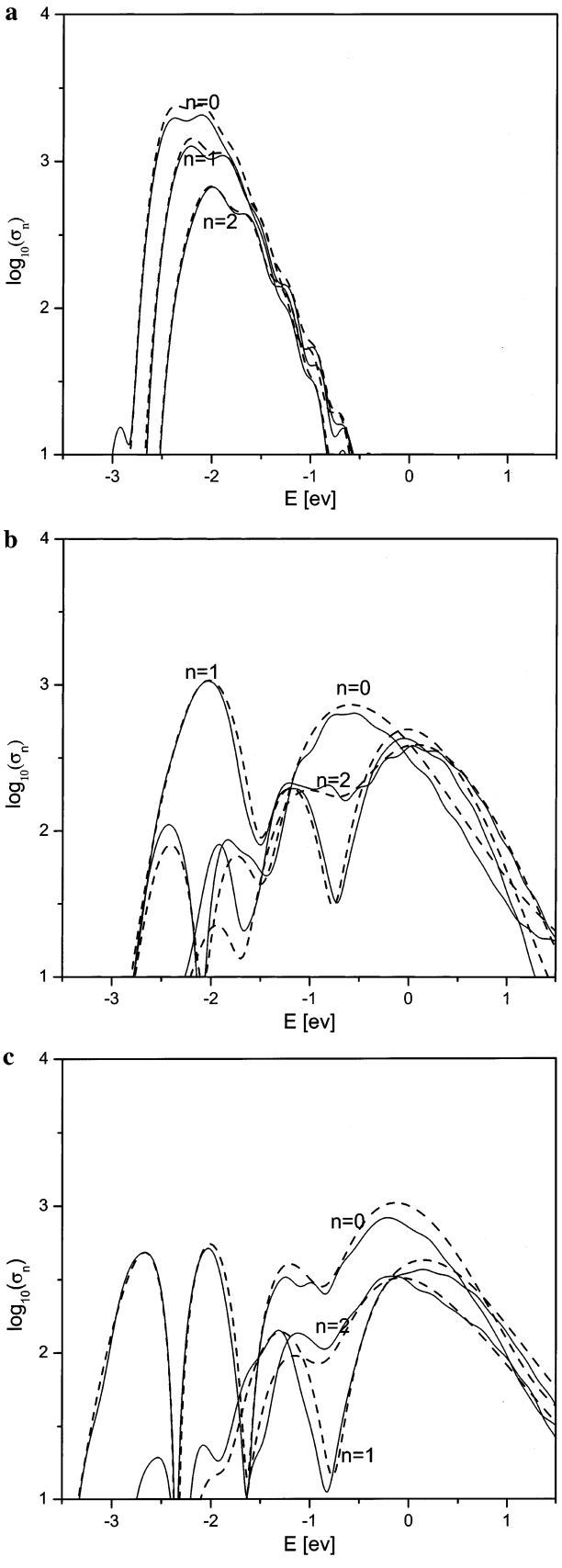

Figure 3. Partial photodissociation cross sections for the $|00^+\rangle$, $|31^-\rangle$, and $|40^-\rangle$ vibrational states of H_2O, are shown in panels a−c, respectively. Results for the final vibrational states $n = 0$, 1, and 2 of the OH photofragment are displayed. Partial photodissociation cross sections are displayed in arbitrary units and logarithmic scale to facilitate the comparison between semiclassical (solid lines) and quantum results (dahsed lines).

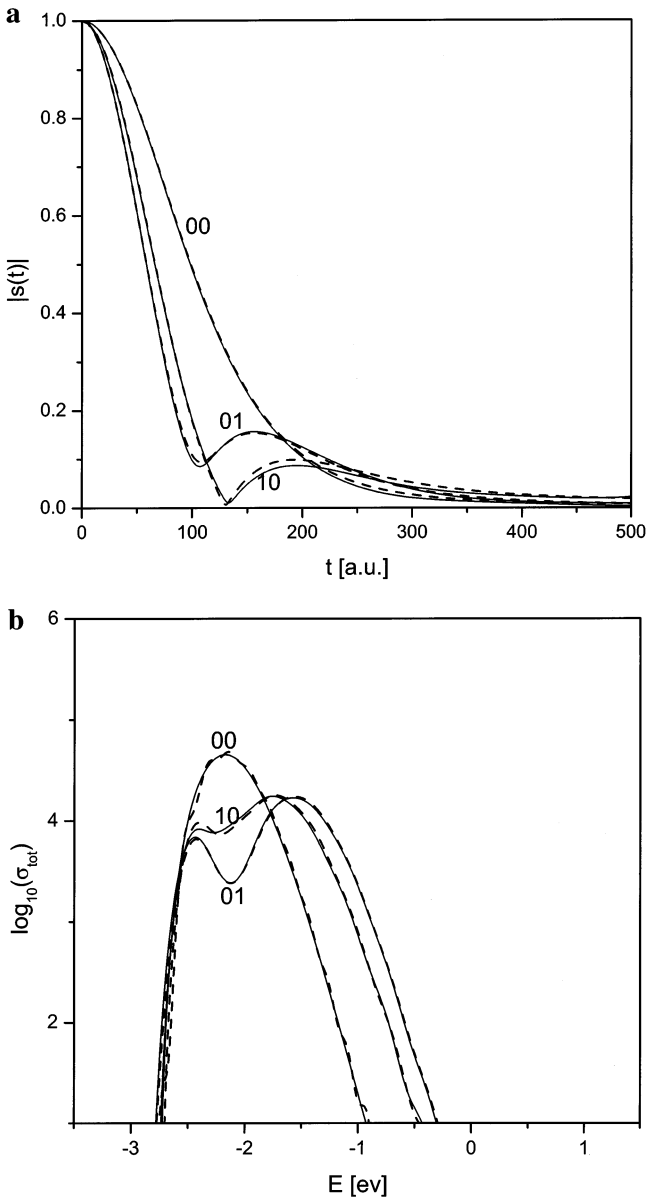

Figure 4. (a) Comparison between semiclassical (solid lines) and quantum results (dashed lines) for the modulus of the survival amplitudes associated with the DOH molecule initially prepared in the $|00^+\rangle$, $|01^-\rangle$, and $|10^-\rangle$ vibrational states. Panel b compares of the semiclassical (solid lines) and quantum results (dashed lines) for the corresponding total photodissociation cross sections as a function of the energy $E = E_j + \hbar\omega$ in the excited electronic state. Photodissociation cross sections are in arbitrary units and displayed in logarithmic scale to facilitate the comparison.

= 1). Both calculations also predict that at higher energies the vibrational distributions for both initial states become rather broad. These results are also in excellent agreement with previous quantum calculations (see Figure 5 of ref 15). In contrast, previous SC-IVR computations of partial photodissocation cross sections were in poor agreement with quantum results (see Figure 4 of ref 16, where the $n = 2$ cross section exceeds the $n = 1$ cross section near $E = -1.94$ eV, and the semiclassical peak is shifted to lower energy).

For completeness, Figure 4a compares the semiclassical (solid lines) and quantum (dashed lines) results for the modulus of the survival amplitudes associated with the DOH molecule, initially prepared in the $|00^+\rangle$, $|01^-\rangle$, and $|10^-\rangle$ vibrational states. The comparison of the corresponding total photodissociation cross sections, as a function of the energy $E = E_j + \hbar\omega$ in the

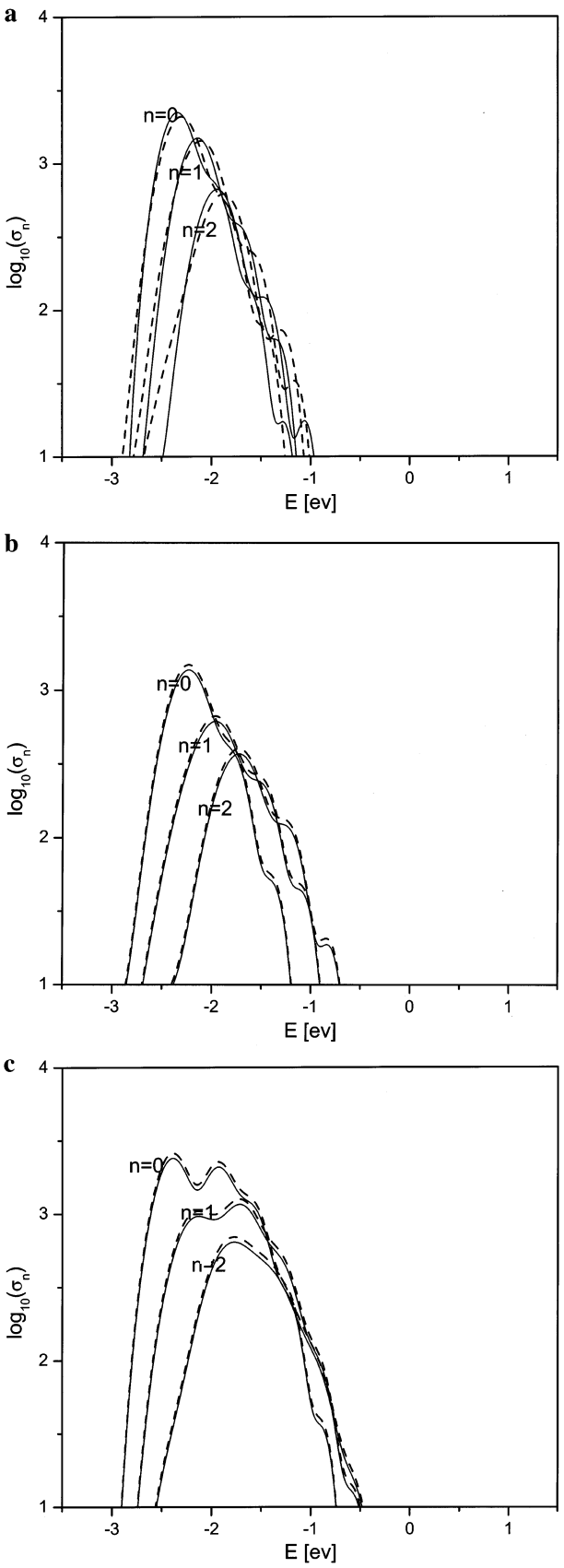

Figure 5. Partial photodissociation cross sections for the $|00^+\rangle$, $|01^-\rangle$, and $|10^-\rangle$ vibrational states of HOD, are shown in panels a−c, respectively. Results are shown for the final vibrational states $n = 0$, 1, and 2 of the OH photofragment. Partial photodissociation cross sections are displayed in arbitrary units and logarithmic scale to facilitate the comparison between semiclassical (solid lines) and quantum results (dahsed lines).

excited electronic state, is presented in Figure 4b. Once again we find excellent agreement between semiclassical and full quantum mechanical calculations. Remarkably, the TS SC-IVR is able to describe not only the effects of isotopic substitution but also *all* the differences between the total photodissociation cross sections obtained by preparing the HOD molecule in different vibrational states. Excellent agreement between semiclassical and full quantum mechanical results is also observed in the comparison of partial photodissociation cross sections displayed in Figure 5 for the $|00^+\rangle$, $|01^-\rangle$, and $|10^-\rangle$ vibrational states of HOD (see panels a−c, respectively).

IV. Conclusions

In this article we have demonstrated for the first time the capabilities of the TS SC-IVR method of Burant and Batista to the description of a real application reaction: the photodissociation dynamics of H_2O in the (A^1B_1) band.

Our semiclassical results were able to reproduce the correct structure of survival amplitudes as well as the detailed partial and total photoabsorption cross sections as functions of the photoexcitation energy. We have demonstrated that the TS SC-IVR describes *all* the features associated with the H_2O and DOH photodissociation dynamics in excellent agreement with full quantum calculations, including the detailed description of the vibrational state distributions of OH photofragments produced after photoexcitation of nearly degenerate states in the highly excited vibrational H_2O. This was not a surprise because the TS SC-IVR method was designed to approach the quantum mechanical calculations both formally and numerically, but demonstrated the potentiality of the methodology for studying photodissociation reactions of polyatomic systems, even when the outcome of the photochemical reaction was highly sensitive to the initial quantum state of the system.

In the spirit of the original SC-IVR formulation, the quantum mechanical propagator is computed by propagating classical trajectories that are independent of each other. However, contrary to the original formulation, the time evolution operator is obtained by concatenating finite time propagators. The accuracy is therefore significantly improved, as demonstrated by the comparison of our results with full quantum mechanical calculations and the results obtained by earlier SC-IVR studies.

Acknowledgment. We are grateful to John Tully for many enjoyable conversations, and for his always helpful and thoughtful advice. V.S.B. acknowledges a generous allocation of supercomputer time from the National Energy Research Scientific Computing Center and financial support for this work from the Provost's office at Yale University.

References and Notes

(1) Burant, J.; Batista, V. *J. Chem. Phys.* **2002**, *116*, 2748.
(2) Andresen, P.; Schinke, R. In *Molecular Photodissociation Dynamics*; Ashfold, M., Baggott, J., Eds.; Royal Society of Chemistry: London, 1987; Chapter 3.
(3) Staemmler, V.; Palma, A. *Chem. Phys.* **1985**, *93*, 63.
(4) Engel, V.; Schinke, R.; Staemmler, V. *J. Chem. Phys.* **1988**, *88*, 129.
(5) Wang, H.-T.; Felps, W.; McGlynn, S. *J. Chem. Phys.* **1977**, *67*, 2614.
(6) Andresen, P.; Ondrey, G.; Titze, B.; Rothe, E. *J. Chem. Phys.* **1984**, *80*, 2548.
(7) Andresen, P.; Beushausen, V.; Hausler, D.; Lulf, H. *J. Chem. Phys.* **1985**, *83*, 1429.
(8) Hausler, D.; Andresen, P.; Schinke, R. *J. Chem. Phys.* **1987**, *87*, 3949.
(9) Kuhl, K.; Schinke, R. *Chem. Phys. Lett.* **1989**, *158*, 81.
(10) Sension, R.; Brudzynski, R.; Hudson, B. *Phys. Rev. Lett.* **1988**, *61*, 694.

(11) Shafer, N.; Satyapal, S.; Bersohn, R. *J. Chem. Phys.* **1989**, *90*, 6807.
(12) Guo, H.; Murrell, J. *Mol. Phys.* **1988**, *65*, 821.
(13) Engel, V.; Schinke, R. *J. Chem. Phys.* **1988**, *88*, 6831.
(14) Hennig, S.; Engel, V.; Schinke, R. *Chem. Phys. Lett.* **1988**, *149*, 455.
(15) Weide, K.; Hennig, S.; Schinke, R. *J. Chem. Phys.* **1989**, *91*, 7630.
(16) Campolieti, G.; Brumer, P. *J. Chem. Phys.* **1997**, *107*, 791.
(17) Vanderwal, R.; Crim, F. *J. Phys. Chem.* **1989**, *93*, 5331.
(18) Miller, W. H. *J. Chem. Phys.* **1970**, *53*, 3578.
(19) Miller, W. *J. Phys. Chem. A* **2001**, *105*, 2942−2955.
(20) Bonella, S.; Coker, D. *J. Chem. Phys.* **2001**, *114*, 7778.
(21) Bonella, S.; Coker, D. *Chem. Phys.* **2001**, *268*, 189.
(22) Yang, G.; Herman, M. *J. Phys. Chem. B* **2001**, *105*, 6562.
(23) Gelabert, R.; Giménez, X.; Thoss, M.; Wang, H.; Miller, W. *J. Chem. Phys.* **2001**, *114*, 2572−2579.
(24) Sun, X.; Miller, W. H. *J. Chem. Phys.* **1997**, *106*, 916−927.
(25) Campolieti, G.; Brumer, P. *Phys. Rev. A* **1994**, *50*, 997.
(26) Campolieti, G.; Brumer, P. *J. Chem. Phys.* **1992**, *96*, 5969.
(27) Walton, A.; Manolopoulos, D. *Mol. Phys.* **1996**, *87*, 961−978.
(28) Herman, M. F. *Chem. Phys. Lett.* **1997**, *275*, 445.
(29) Kay, K. G. *J. Chem. Phys.* **1994**, *100*, 4377−4392.
(30) Kay, K. G. *J. Chem. Phys.* **1994**, *100*, 4432−4445.
(31) Kay, K. G. *J. Chem. Phys.* **1994**, *101*, 2250−2260.
(32) Brewer, M. L.; Hulme, J. S.; Manolopoulos, D. E. *J. Chem. Phys.* **1997**, *106*, 4832−4839.
(33) Ovchinnikov, M.; Apkarian, V. A. *J. Chem. Phys.* **1998**, *108*, 2277.
(34) Sun, X.; Miller, W. H. *J. Chem. Phys.* **1998**, *108*, 8870.
(35) Batista, V. S.; Miller, W. H. *J. Chem. Phys.* **1998**, *108*, 498−510.
(36) Batista, V.; Zanni, M.; Greenblatt, B.; Neumark, D.; Miller, W. *J. Chem. Phys.* **1999**, *110*, 3736−3747.
(37) Guallar, V.; Batista, V.; Miller, W. *J. Chem. Phys.* **1999**, *110*, 9922−9936.
(38) Guallar, V.; Batista, V.; Miller, W. *J. Chem. Phys.* **2000**, *113*, 9510−9522.
(39) Batista, V. S.; Brumer, P. *J. Chem. Phys.* **2001**, *114*, 10321.
(40) Batista, V.; Brumer, P. *J. Phys. Chem. A* **2001**, *105*, 2591.
(41) Miller, W. *J. Chem. Phys.* **1991**, *95*, 9428−9430.
(42) Heller, E. *J. Chem. Phys.* **1991**, *95*, 9431.
(43) Heller, E. *J. Chem. Phys.* **1981**, *75*, 2923−2931.
(44) Heller, E. *Chem. Phys. Lett.* **1975**, *34*, 321−325.
(45) Huber, D.; Heller, E. J. *J. Chem. Phys.* **1988**, *89*, 4752.
(46) Huber, D.; Ling, S.; Imre, D.; Heller, E. *J. Chem. Phys.* **1989**, *90*, 7317−7329.
(47) Grossmann, F. *Phys. Rev. Lett.* **2000**, *85*, 903−907.
(48) Andersson, L. *J. Chem. Phys.* **2001**, *115*, 1158−1165.
(49) Shalashilin, D.; Child, M. *J. Phys. Chem.XXXX* **2001**, *115*, 5367.XXXX
(50) Shalashilin, D.; Child, M. *J. Phys. Chem.XXXX* **2001**, *114*, 9296.XXXX
(51) Shalashilin, D.; Jackson, B. *Chem. Phys. Lett.* **2000**, *318*, 305.
(52) Herman, M. F.; Kluk, E. *Chem. Phys.* **1984**, *91*, 27−34.
(53) Colbert, D.; Miller, W. *J. Chem. Phys.* **1992**, *96*, 1982.
(54) Sorbie, K.; Murrell, J. *Mol. Phys.* **1975**, *29*, 1387.
(55) Halonen, L.; Carrington, T. *J. Chem. Phys.* **1988**, *88*, 4171.
(56) Balint-Kurti, G.; Nixon, R.; Marston, C. *J. Chem. Soc., Faraday Trans.* **1990**, *86*, 1741.
(57) Galant, D. G. D. *J. Quant. Spectrosc. Radiat. Transfer* **1992**, *47*, 391.
(58) Kosloff, D.; Kosloff, R. *J. Comput. Phys.* **1983**, *52*, 35.